A&A 678, A100 (2023)
https://doi.org/10.1051/0004-6361/202346400

Astronomy & Astrophysics

Quasi-periodic oscillation detected in γ-rays in blazar PKS 0346−27

Raj Prince[1], Anuvab Banerjee[2], Ajay Sharma[2], Avik Kumar das[3], Alok C. Gupta[4,5], and Debanjan Bose[6]

[1] Center for Theoretical Physics, Polish Academy of Sciences, Al. Lotników 32/46, 02-668 Warsaw, Poland
e-mail: raj@cft.edu.pl
[2] S. N. Bose National Centre for Basic Sciences, Block JD, Salt Lake, Kolkata 700106, India
[3] Department of Physical Sciences, Indian Institute of Science Education and Research Mohali, Knowledge City, Sector 81, SAS Nagar, Punjab 140306, India
[4] Key Laboratory for Research in Galaxies and Cosmology, Shanghai Astronomical Observatory, Chinese Academy of Sciences, Shanghai 200030, PR China
[5] Aryabhatta Research Institute of Observational Sciences (ARIES), Manora Peak, Nainital 263001, Uttarakhand, India
[6] School of Astrophysics, Presidency University, 86/1 College Street, Kolkata 700073, West Bengal, India

Received 13 March 2023 / Accepted 20 August 2023

ABSTRACT

Aims. We present a variability study of the blazar PKS 0346−27 conducted between December 2018 and January 2022 using archival γ-ray observations from *Fermi*-LAT.
Methods. We used Lomb–Scargle periodogram and weighted wavelet transform methods to detect the presence of periodicity or quasi-periodicity and localize this feature in time and frequency space. We estimated the significance of the periodicity feature using a Monte Carlo simulation approach. We also determined the global significance of the periodicity to test the robustness of our claim. To explore the most probable scenario, we modeled the light curve with both a straight-jet and a curved-jet model.
Results. We detect a periodicity feature of ∼100 days in the entire period of observation with a statistical significance of 3σ, which amounts to a 99.7% confidence level. The global significance of this feature is found to be 96.96%. Based on the Akaike information criterion, the most probable explanation is that the observed emission is enhanced due to the helical motion of a blob within a curved jet.
Conclusions. The origin of this quasi-periodic oscillation is very likely a region of enhanced emission moving helically inside a curved jet. This work presents strong evidence for jet curvature in the source and an independent (albeit a little serendipitous) procedure to estimate the curvature in blazar jets.

Key words. galaxies: active – BL Lacertae objects: individual: PKS 0346−27 – BL Lacertae objects: general – gamma rays: galaxies

1. Introduction

Active galactic nuclei (AGNs) are believed to derive their ultimate power from accretion onto a supermassive black hole (SMBH) with a mass in the range 10^6–10^{10} $M_\odot$. Blazar variability can be sufficiently characterized as a red-noise process. In the time series data, or light curves (LCs), quasi-periodic oscillations (QPOs) appear to be rare for AGNs (for a review, see Gupta 2018). There have been some strong claims of AGN QPOs in different bands of the electromagnetic (EM) spectrum with diverse periods (e.g., Gierliński et al. 2008; Gupta et al. 2009, 2018, 2019; Lachowicz et al. 2009; Lin et al. 2013; King et al. 2013; Alston et al. 2014, 2015; Sandrinelli et al. 2014, 2016, 2017; Graham et al. 2015; Ackermann et al. 2015; Pan et al. 2016; Bhatta 2019; Sarkar et al. 2021; Roy et al. 2022a; Jorstad et al. 2022; Das et al. 2023, and references therein). However, many of the claimed QPOs, particularly claims made before 2008, are marginal detections, lasting only a few cycles, and the originally quoted statistical significance is probably overestimated (for a review, see Gupta 2014). In the last 15 years or so, there have been very few strong claims of QPO detections in blazars in different bands of the EM spectrum (and on diverse timescales; e.g., Gupta et al. 2009, 2019; Lachowicz et al. 2009; King et al. 2013; Graham et al. 2015; Ackermann et al. 2015; Zhou et al. 2018a; Bhatta 2019; Sarkar et al. 2021; Roy et al. 2022a; Jorstad et al. 2022; Das et al. 2023, and references therein) or in other subclasses of AGNs in X-ray bands (e.g., Gierliński et al. 2008; Alston et al. 2014, 2015; Pan et al. 2016; Gupta et al. 2018; Agarwal et al. 2021, and references therein).

Regarding *Fermi*-LAT blazar observations, QPOs in a few blazars have been detected on diverse timescales, for example: a ∼34.5-day QPO in PKS 2247−131 (Zhou et al. 2018a), a ∼71-day QPO in B2 1520+31 (Gupta et al. 2019), a ∼47-day QPO in 3C 454.3 (Sarkar et al. 2021), and ∼3.6-day and ∼92-day QPOs in different segments of the LC of PKS 1510−089 (Roy et al. 2022b). The first γ-ray QPO was detected in blazar PG 1553+113 by Ackermann et al. (2015) and Tavani et al. (2018). The QPO period was found to be ∼2.18 years. γ-ray QPOs on different timescales were also detected in many other blazars, such as PKS 2155−304 (1.73 years; Sandrinelli et al. 2014; Zhang et al. 2017a), PKS 0426−380 (3.35 years), and PKS 0301−243 (2.1 years; Zhang et al. 2017c,b). A systematic search for QPOs in the γ-ray LCs of blazars (FSRQs and BL Lacs) is presented in Ren et al. (2023), who detected a range of timescales, from months to years. A small sample of blazars was also explored by Bhatta & Dhital (2020), in which QPOs in γ-ray LCs are found to have durations of a few hundred days. Most interestingly, all γ-ray QPOs detected in blazars have periods in the range of a few tens of days up to, in some cases, a year (Ren et al. 2023), and all blazars are Flat Spectrum Radio

Quasars (FSRQs). This is possibly evidence of the fundamental behavior of FSRQs that show γ-ray QPOs with these periods but a more systematic study is required.

PKS 0346−27 is an FSRQ blazar at redshift $z = 0.991$ (White et al. 1988). The source has been detected in different EM bands (Kamaram et al. 2023) and recently also discovered as a γ-ray emitter and listed in the *Fermi*-LAT Fourth Source Catalog (4FGL; Abdollahi et al. 2020). The mass of the SMBH at the center of PKS 0346−27 was estimated, via multiwavelength spectral energy distribution (SED) modeling in the low flux state of the source, to be $\sim 2 \times 10^8\ M_\odot$ (Angioni et al. 2019). Via multiwavelength observations, the source has been detected in the high activity state in the optical to near-infrared (Nesci 2018a) as well as in UV and X-ray regions (Nesci 2018b). Via a multiwaveband spectral investigation of quiescent and flaring phases using a one-zone leptonic model, this source was identified as an intermediate synchrotron peaked (ISP) blazar (Angioni et al. 2019). A detailed broadband SED modeling of the source was done by Kamaram et al. (2023), who modeled the broadband SED with a combination of external Compton from the accretion disk and the broad-line region.

The presence of QPOs in the LCs of AGNs is of great importance and can provide strong support for the common nature of the accretion processes onto black holes ranging from a few solar masses up to the SMBHs present in AGNs (Abramowicz & Kluźniak 2001; Remillard & McClintock 2006; Zhou et al. 2015). Possible AGN emission models that might explain QPOs in AGNs in different EM bands on diverse timescales have been discussed in a series of works (e.g., Gierliński et al. 2008; Gupta et al. 2009; Lachowicz et al. 2009; Pan et al. 2016; Sarkar et al. 2021; Roy et al. 2022a; Jorstad et al. 2022; Das et al. 2023, and references therein).

The paper is organized as follows. In Sect. 2 we briefly introduce the *Fermi*-LAT γ-ray data and present its analysis. In Sect. 3 we describe the various QPO analysis techniques and the results we obtained. A discussion and our conclusions are given in Sect. 4.

2. Data reduction

We used the standard `Fermitools` package to extract and analyze the *Fermi*-LAT data in 0.1–300 GeV for the period between MJD 58480 and 59598. A 10° region of interest (ROI) was chosen around the source to extract the photon flux. The user-specified constraints `'evclass=128'` and `'evtype=3'`, corresponding to the `gtselect` tool, were applied to select rows from the input event data. A zenith angle cut of 90° was applied to filter out any plausible contamination from the Earth's limb. The recent 4FGL DR3 catalog was used to produce the source model.xml file, and the source best-fit parameters were obtained using the maximum likelihood. The recent instrument response function `P8R3_SOURCE_V3` was applied for the analysis. In order to account for the isotropic and the diffuse background emission, `iso_P8R3_SOURCE_V3_v1.txt` and `gll_psc_v31.fits` were employed, respectively, which are available from the *Fermi* Science Support Center (FSSC). We also identified the sources with low test statistics (TS < 9) and excluded them from further analysis. We fixed all the other parameters of other sources within the ROI and optimized the source-of-interest parameters with a maximum likelihood to obtain the flux in the defined time bin. We also estimated the TS value of each data point in the LC and again applied the condition of TS < 9 to remove the low photon statistics points.

3. Light curve analysis and results

The γ-ray LC of PKS 0346−27 in the energy range 0.1–300 GeV obtained from *Fermi*-LAT is displayed in Fig. 1 (lower panel), which shows a clear flux modulation in the period MJD 58480 to 59598. In the top panel, we present the full LC starting from August 5, 2008 (MJD = 54683), but we can see that, for most of the time, the source is in a quiescent phase and starts to show flux variability only after December 2018. The green-shaded region represents the period we analyzed, when the high flux state of the source, as well as variability features, are persistently observed for a duration of >3 years. In order to quantify such periodic modulation, we used independent QPO analysis techniques: the Lomb–Scargle periodogram (LSP) and weighted wavelet Z-transform (WWZ) methods.

3.1. Lomb–Scargle periodogram and testing the QPO significance

The LSP method is one of the most widely used to identify the periodicities in time series (Scargle 1982). The advantage of the LSP over the standard discrete Fourier transform method is that in the case of LSP, the data gaps and data collection irregularities are accounted for by the least-square fitting of the sinusoidal waves of the form $X(t) = A \cos \omega t + B \sin \omega t$. Such a fitting procedure reduces the effect of the noise component and provides a correct measure of the detected periodicity (Zhang et al. 2017a,b).

Red-noise-type variability features in temporal frequency is a hallmark of AGNs and blazar sources. The periodogram is typically represented by a power spectral density (PSD) of the form $P(\nu) \sim A\nu^{-\beta}$, where ν represents the temporal frequency and $\beta > 0$ represents the spectral slope. Owing to such a power-law profile, the high amplitude features in the LSP detected on longer timescales (i.e., within the low-frequency domain) could appear to be a genuine periodicity feature (Timmer & Koenig 1995; Max-Moerbeck et al. 2014). Owing to the presence of such a red-noise feature, a rigorous estimation of the significance of periodogram peaks must be done before concluding as to whether a peaked feature is a true QPO. We carried out the significance test by using the power spectral response (PSRESP; Uttley et al. 2002) method, which is widely used for AGNs and blazars (Chatterjee et al. 2008). The red-noise PSDs of blazar LCs are typically well represented by a power-law or a bending power-law feature (Vaughan 2005). Therefore, we used a bending power law and a log-normal model to respectively fit the PSD and probability density function (PDF) of the original LC. A total of 1000 LCs with the same PSD and PDF as that of the original LC were simulated using the `DELightcurveSimulation`[1] code. Using this procedure, we observe an evident peak at ∼100 days with $\sim 3\sigma$ significance.

3.2. Weighted wavelet Z-transform

Another commonly used method of periodicity detection in blazar LCs is the wavelet transform method (Bhatta et al. 2013, 2016; Das et al. 2023). This approach attempts to determine the presence of any periodicity feature by fitting the data with a sinusoidal wave function. The localization of the waves in both time and frequency space is possible in this context and allows one to explore the evolution of QPO features with time (Foster 1996).

[1] https://github.com/samconnolly/DELightcurveSimulation

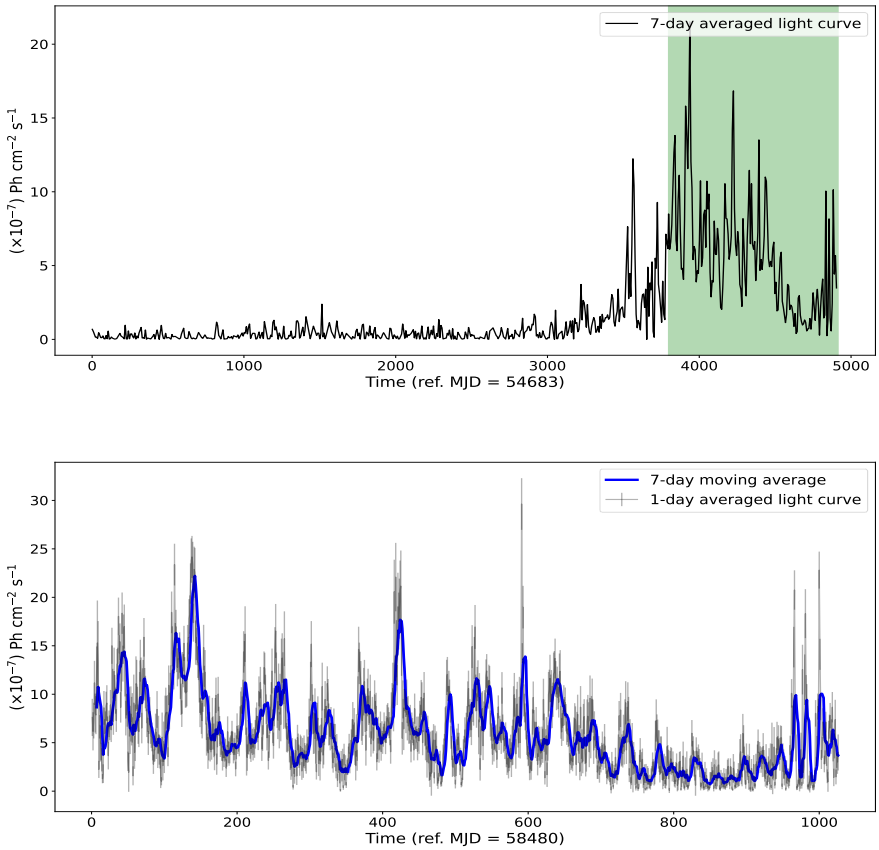

Fig. 1. Long-term γ-ray LC for PKS 0346−27. For the majority of the time, the source was in the quiescent phase; it showed substantial flaring activity and a steady high flux state after December 2018. Upper panel: seven-day-binned LC between August 5, 2008 (MJD = 54 683) and January 19, 2023 (MJD = 59 598). The high flux state, marked with a light green patch (MJD = 58 480 to 59 598), is the period in which we searched for QPOs. Lower panel: one-day-binned *Fermi*-LAT LC in 0.1–300 GeV for the full domain of observation between MJD = 58 480 and 59 598. We superimpose the seven-day moving average on top of the LC to make the periodic modulation explicit. An oscillatory feature is clearly visible in the LC.

It is a powerful tool for determining whether such oscillations gradually develop, evolve in frequency space, and gradually dissipate over time.

In brief, the WWZ method convolves a LC with a time- and frequency-dependent kernel and decomposes the data into time and frequency domains to create a WWZ map. We used the Morlet kernel (Grossmann & Morlet 2009), which has the functional form

$$f[\omega(t-\tau)] = \exp[i\omega(t-\tau) - c\omega^2(t-\tau)^2]. \quad (1)$$

The corresponding WWZ map is

$$W[\omega,\tau;x(t)] = \omega^{1/2}\int x(t)f^*[\omega(t-\tau)]\mathrm{d}t, \quad (2)$$

where f^* is the complex conjugate of the Morlet kernel, f, and τ and ω are respectively the time and frequency shift. This kernel serves as a windowed discrete Fourier transform that contains a frequency-dependent window of size $\exp -c\omega^2(t-\tau)^2$. The WWZ map has the advantage of being able to detect statistically significant periodicities, as well as the time spans of their persistence.

Our WWZ analysis revealed a prominent peak at ∼100 days that was present throughout the entire studied period. This is evident from the presence of a significant power concentration within a narrow frequency window for the full domain of observation, as shown in the right panel of Fig. 2. We also detected a broader peak in the WWZ map at ∼50 days, but it is only present for a short period of time and is well below the 3σ significance in the LSP method.

To verify the veracity of the QPO in the LC, we tested the significance of each peak. The significance, determined using the PSRESP method, is $>3\sigma$ (Fig. 2).

4. Discussion and conclusion

Several different physical models could explain the emergence of periodicity or quasi-periodicity in blazar LCs. One plausible explanation is a binary SMBH AGN system. According to this model, when the secondary black hole pierces the primary black hole's accretion disk during orbit, a QPO may be detected (Valtonen et al. 2008). This model is explicitly given for the blazar OJ 287, for which the mass of the binary SMBH system is much larger and the period is ∼12 years (Valtonen et al. 2008). So, this model is unlikely to explain the detected QPO in the present work. Another possible explanation is the rotation of the accretion disk hot-spot or spiral shocks or some other non-axisymmetric phenomena around the innermost region of the accretion disk. This will primarily manifest in the optical/X-ray domain; periodicity in γ-ray photons could be observed via external Compton scattering. The central SMBH mass corresponding to this phenomenon happens to be (Gupta et al. 2009)

$$\frac{M}{M_\odot} = \frac{3.23\times10^4 P}{(r^{3/2}+a)(1+z)}, \quad (3)$$

where P is the orbital period in seconds, and z is the redshift of the object. The central SMBH mass can be roughly estimated in the case of a Schwarzschild black hole (with $r = 6.0$ and $a = 0$) and for a maximal Kerr black hole (with $r = 1.2$ and $a = 0.9982$; Gupta et al. 2009). In our case, considering the 100-day period, we find the central SMBH mass to be $9.48\times10^9\,M_\odot$ in the Schwarzschild scenario and $6.01\times10^{10}\,M_\odot$ in the extreme Kerr scenario. The former estimate is quite large, and the latter essentially exceeds all other SMBH mass estimates. Therefore, it is rather unlikely that the variability feature is directly reflective of some rotating axisymmetric phenomena.

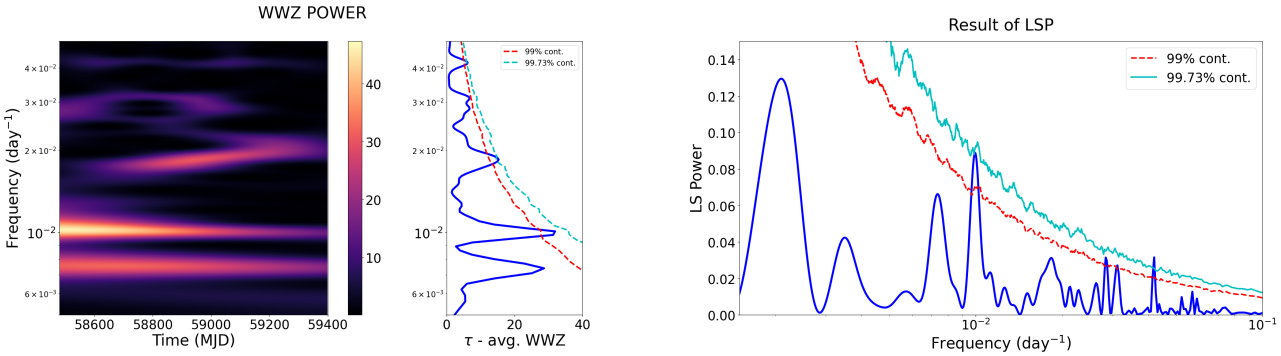

Fig. 2. Plausible detection of the QPO feature corresponding to the LC shown in the bottom panel in Fig. 1. Right panel: LSP with the statistical significance of the LSP peak, along with the average WWZ map. The observed 0.01-day^{-1} peak is ∼3σ significant. The average WWZ map shows a distinct peak at this frequency as well, strongly suggesting the presence of a QPO feature. Left panel: WWZ map and the time-averaged power. A distinct concentration of power within a narrow frequency band of around 100 days (0.01 days^{-1}) is observed. A 99.0% and a 99.73% significance are estimated for the LSP and WWZ results, respectively, which are shown in red and cyan.

A magnetohydrodynamic origin of QPOs on a timescale of weeks to months driven by kink instabilities in the jet spine has recently been proposed by Dong et al. (2020). However, they also observed an anti-correlation between the optical polarization degree and the flux. At present, there is not enough well-sampled optical polarization degree data to be able to verify this scenario.

Transient QPOs can also arise from a strong turbulent flow occurring behind a propagating shock or a standing shock in the jet (Marscher et al. 1992). The dominant turbulent cell, which can exhibit enhanced Doppler boosting, introduces a QPO component to the observed LC at the turnover period of the cell. In our case, this turnover period is ∼500 days (assuming a Doppler factor = 10.0), suggesting the presence of a very large eddy, which would be necessary to explain the observed QPO. Furthermore, due to the stochastic nature of the cell, it is highly likely that the QPO would not persist for many cycles (Wiita 2011).

Since the blazar emission is jet-dominated, it is likely that the variability signatures have some connection with the jet emission characteristics. In the case of a precessing jet, quasi-periodic variability signatures would be clearly observed as a consequence of varying Lorentz factors along the line of sight of the observer. The jet precession could be induced by the presence of a secondary SMBH in a blazar, resulting in a binary SMBH system (Valtonen et al. 2008; Graham et al. 2015). It could also be induced if there is a Lense-Thirring precession of the disk (Fragile & Meier 2009), which would in turn influence the jet orientation. However, it has been suggested that such dynamical mechanisms would produce physical periods of ∼1−2 years (Rieger 2007), which is well above the periodicity we have observed in our case.

Jet-induced quasi-periodicity could also originate from the motion of plasma blobs along the internal helical structure of the jet, as shown in Fig. 3. The variation in the Doppler boosting factor as a consequence of the variation in the viewing angle of the plasma blob would lead to quasi-periodic variability features (Mohan & Mangalam 2015). Depending on the Doppler boosting factor and the viewing angle, the period of variability could range from around a few days to a few months. The periodicity that we have detected falls within this range. In this scenario, the blob can produce γ-ray emission via external Compton and synchrotron self-Compton processes (one-zone leptonic scenario). For a blob moving helically, the changing viewing angle

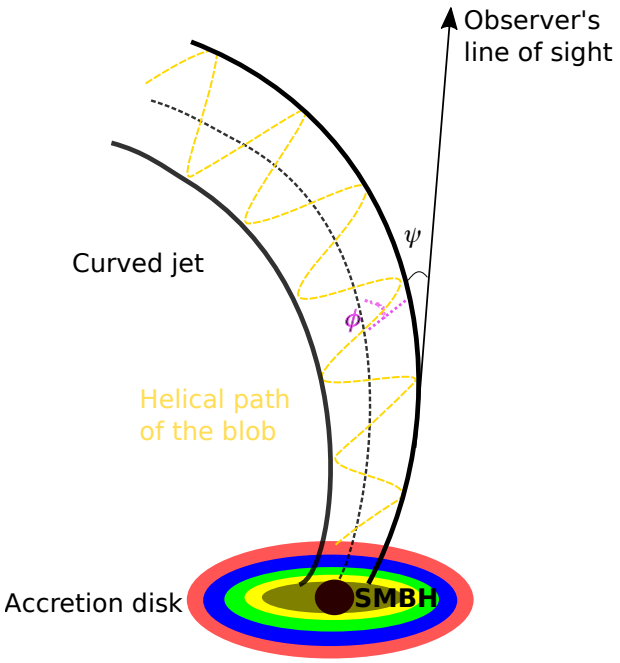

Fig. 3. Possible curved-jet present in the source. The ϕ is the angle between the blob velocity vector and the jet axis. The ψ is the viewing angle measured between the jet axis and the observer's line of sight. Note that the accretion disk is represented by the multicolor blackbody and that the image is not to scale.

of the blob with respect to our line of sight, $\cos\theta(t)$, is given by (Zhou et al. 2018b)

$$\cos\theta(t) = \cos\phi\cos\psi + \sin\phi\sin\psi\cos(2\pi t/P_{\rm obs}), \quad (4)$$

where $P_{\rm obs}$ is the observed period and ϕ is the pitch angle defined between the blob velocity vector and the jet axis. The ψ is the viewing angle, or inclination angle, measured between the observer's line of sight and the jet axis. As the observer, we see a boosted emission in γ-rays with Doppler factor δ, and hence the observed period in the blob frame can be translated as $P_{\rm obs} = (1 - \beta\cos\psi\cos\phi)\ P'$, where $P_{\rm obs}$ is the observed period and the P is the period in the blob frame. Given standard blazar parameters (ψ and ϕ), we can estimate the period in the blob rest frame. For an FSRQ-type blazar, the Lorentz factor

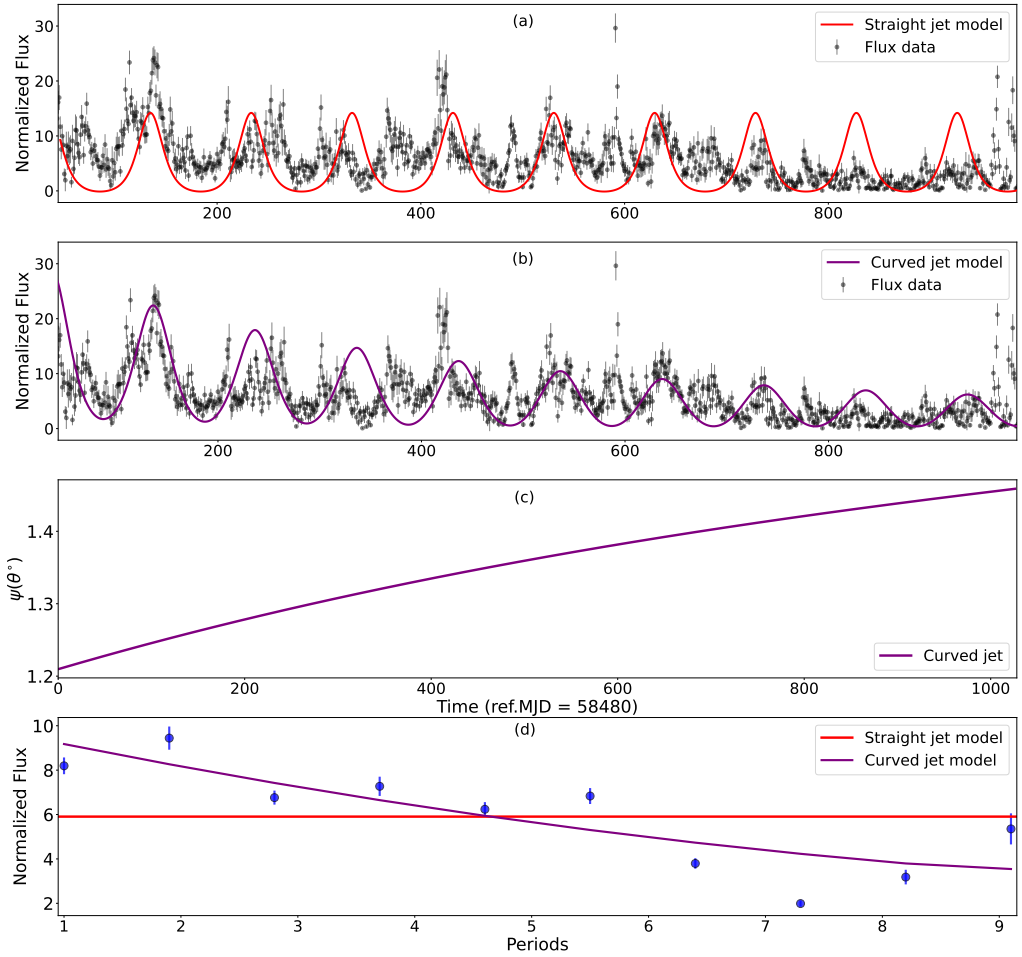

Fig. 4. γ-ray LC of PKS 0346−27 modeled using two different jet scenarios: (a) a straight-jet model (red) and (b) a curved-jet model (purple), shown with modulation of 100 days. The black data points represent the observed γ-ray flux. (c) Viewing angle of the jet shown as a function of time (t). (d) Average flux in each period modeled using both the straight and curved-jet models. The analysis of the AIC strongly supports the curved-jet scenario as the favored explanation for the observed γ-ray emission within the given time domain. The straight-jet model yielded an AIC value of 17.85, while the curved-jet model yielded an AIC value of 10.15.

is chosen as $\Gamma = 15$, $\phi = 2°$, and $\psi = 5°$. Using the expression $\Gamma = 1/\sqrt{1-\beta^2}$, β is estimated to be 0.99777 and the QPO period in the blob rest frame is found to be $P' = 41.5$ years. Along the helical path in the jet, the distance traveled by the blob in one cycle is given by $D_1 = c\beta P \cos\phi \approx 12.63$ pc. The modified helical jet model introduces a significant departure from the conventional understanding of a straight jet, where the inclination angle of the jet's axis remains constant with respect to the line of sight. In this modified model, the blob exhibits helical motion within a curved jet, where the viewing angle $\psi \equiv \psi(t)$ (Sarkar et al. 2021) varies as a function of time. By incorporating the dependence of the viewing angle on time, expressed as $\cos(\theta_{\rm obs}(t))$, into the Doppler factor $\delta = 1/\Gamma(1-\beta\cos(\theta_{\rm obs}))$, we obtain the following expression for the observed emission ($F_\nu \propto \delta^3$; Sarkar et al. 2021):

$$F_\nu \propto \frac{F'_{\nu'}}{\Gamma^3(1+\sin\phi\sin\psi)^3}\left(1-\frac{\beta\cos\phi\cos\psi}{1+\sin\phi\sin\psi}\cos\left(\frac{2\pi t}{P_{\rm obs}}\right)\right)^{-3}, \quad (5)$$

where $F'_{\nu'}$ is the rest-frame emission and $P_{\rm obs}$ is the observed period. We conducted a comprehensive analysis to model the boosted emission in the observed frame using both a straight-jet model (Fig. 4a) and a curved-jet model (Fig. 4b). Additionally, we investigated the variation in the viewing angle over time (Fig. 4c). From our analysis, based on the Akaike information criterion (AIC; for the straight-jet model, this value is found to be 17.85 and for the curved-jet model, it is 10.15), we find that the curved-jet model provides a more likely explanation for the observed γ-ray emission within the given time domain (Fig. 4d). Notably, including a multiplicative trend allowed us to account for changes in the Doppler factor, which could be attributed to a spatial curvature in the jet. This curvature manifests as a time-dependent change in the viewing angle as the blob moves downstream. A hint of helical structure in the jet is also seen in the Very Long Baseline Interferometry (VLBI) in some blazars, where the parsec-scale core appears to be misaligned with the kiloparsec-scale structure of the jet (Conway & Murphy 1993). In the absence of dense VLBI measurements and comprehensive optical monitoring, our understanding of the viewing angle and jet Lorentz factor of this source is limited. Therefore, we did not attempt to constrain any of the jet-based models that resulted in γ-ray periodicity features. As suggested by the *Fermi* science team, the period modulation in the *Fermi*-LAT LC can also come from the artifacts related to the telescope, such as the precession period of the orbit of the *Fermi* spacecraft. To confirm that our result is not contaminated by this precession period, we checked the LCs of all the nearby sources within the 10° ROI around PKS 0346−27. It turns out that most of the sources within 10° are very faint and barely detected by *Fermi*-LAT. There are very

few that have a reasonable LC. We repeated our analysis on those LCs and did not find any evidence of a periodic nature.

Acknowledgements. We thank the anonymous referee for their constructive criticism. This research makes use of the publicly available data from *Fermi*-LAT obtained from the FSSC data server and distributed by NASA Goddard Space Flight Center (GSFC). R. Prince is grateful for the support of the Polish Funding Agency National Science Centre, project 2017/26/A/ST9/-00756 (MAESTRO 9) and the European Research Council (ERC) under the European Union's Horizon 2020 research and innovation program (grant agreement No. [951549]). A. Sharma is grateful to Prof. Sakuntala Chatterjee at S.N. Bose National Centre for Basic Sciences, for providing the necessary support to conduct this research. A.C.G. is partially supported by the Chinese Academy of Sciences (CAS) President's International Fellowship Initiative (PIFI) (grant no. 2016VMB073).

References

Abdollahi, S., Acero, F., Ackermann, M., et al. 2020, ApJS, 247, 33
Abramowicz, M. A., & Kluźniak, W. 2001, A&A, 374, L19
Ackermann, M., Ajello, M., Albert, A., et al. 2015, ApJ, 813, L41
Agarwal, A., Rani, P., Prince, R., et al. 2021, Galaxies, 9, 20
Alston, W. N., Markeviciute, J., Kara, E., Fabian, A. C., & Middleton, M. 2014, MNRAS, 445, L16
Alston, W. N., Parker, M. L., Markevičiūtė, J., et al. 2015, MNRAS, 449, 467
Angioni, R., Nesci, R., Finke, J. D., Buson, S., & Ciprini, S. 2019, A&A, 627, A140
Bhatta, G. 2019, MNRAS, 487, 3990
Bhatta, G., & Dhital, N. 2020, ApJ, 891, 120
Bhatta, G., Webb, J. R., Hollingsworth, H., et al. 2013, A&A, 558, A92
Bhatta, G., Zola, S., Stawarz, Ł., et al. 2016, ApJ, 832, 47
Chatterjee, R., Jorstad, S. G., Marscher, A. P., et al. 2008, ApJ, 689, 79
Conway, J. E., & Murphy, D. W. 1993, ApJ, 411, 89
Das, A. K., Prince, R., Gupta, A. C., & Kushwaha, P. 2023, ApJ, 950, 173
Dong, L., Zhang, H., & Giannios, D. 2020, MNRAS, 494, 1817
Foster, G. 1996, AJ, 112, 1709
Fragile, P. C., & Meier, D. L. 2009, ApJ, 693, 771
Gierliński, M., Middleton, M., Ward, M., & Done, C. 2008, Nature, 455, 369
Graham, M. J., Djorgovski, S. G., Stern, D., et al. 2015, Nature, 518, 74
Grossmann, A., & Morlet, J. 2009, Decomposition of Hardy Functions into Square Integrable Wavelets of Constant Shape (Princeton: Princeton University Press), 126
Gupta, A. 2018, Galaxies, 6, 1
Gupta, A. C. 2014, A&A, 35, 307
Gupta, A. C., Srivastava, A. K., & Wiita, P. J. 2009, ApJ, 690, 216
Gupta, A. C., Tripathi, A., Wiita, P. J., et al. 2018, A&A, 616, L6
Gupta, A. C., Tripathi, A., Wiita, P. J., et al. 2019, MNRAS, 484, 5785
Jorstad, S. G., Marscher, A. P., Raiteri, C. M., et al. 2022, Nature, 609, 265
Kamaram, S. R., Prince, R., Pramanick, S., & Bose, D. 2023, MNRAS, 520, 2024
King, O. G., Hovatta, T., Max-Moerbeck, W., et al. 2013, MNRAS, 436, L114
Lachowicz, P., Gupta, A. C., Gaur, H., & Wiita, P. J. 2009, A&A, 506, L17
Lin, D., Irwin, J. A., Godet, O., Webb, N. A., & Barret, D. 2013, ApJ, 776, L10
Marscher, A. P., Gear, W. K., & Travis, J. P. 1992, in Variability of Blazars, ed (Valtonen: E. Valtaoja & M), 85
Max-Moerbeck, W., Richards, J. L., Hovatta, T., et al. 2014, MNRAS, 445, 437
Mohan, P., & Mangalam, A. 2015, ApJ, 805, 91
Nesci, R. 2018a, ATel, 11269, 1
Nesci, R. 2018b, ATel, 11455, 1
Pan, H.-W., Yuan, W., Yao, S., et al. 2016, ApJ, 819, L19
Remillard, R. A., & McClintock, J. E. 2006, ARA&A, 44, 49
Ren, H. X., Cerruti, M., & Sahakyan, N. 2023, A&A, 672, A86
Rieger, F. M. 2007, Ap&SS, 309, 271
Roy, A., Chitnis, V. R., Gupta, A. C., et al. 2022a, MNRAS, 513, 5238
Roy, A., Sarkar, A., Chatterjee, A., et al. 2022b, MNRAS, 510, 3641
Sandrinelli, A., Covino, S., & Treves, A. 2014, ApJ, 793, L1
Sandrinelli, A., Covino, S., Dotti, M., & Treves, A. 2016, AJ, 151, 54
Sandrinelli, A., Covino, S., Treves, A., et al. 2017, A&A, 600, A132
Sarkar, A., Gupta, A. C., Chitnis, V. R., & Wiita, P. J. 2021, MNRAS, 501, 50
Scargle, J. D. 1982, ApJ, 263, 835
Tavani, M., Cavaliere, A., Munar-Adrover, P., & Argan, A. 2018, ApJ, 854, 11
Timmer, J., & Koenig, M. 1995, A&A, 300, 707
Uttley, P., McHardy, I. M., & Papadakis, I. E. 2002, MNRAS, 332, 231
Valtonen, M. J., Lehto, H. J., Nilsson, K., et al. 2008, Nature, 452, 851
Vaughan, S. 2005, A&A, 431, 391
White, G. L., Jauncey, D. L., Savage, A., et al. 1988, ApJ, 327, 561
Wiita, P. J. 2011, A&A, 32, 147
Zhang, P.-F., Yan, D.-H., Liao, N.-H., & Wang, J.-C. 2017a, ApJ, 835, 260
Zhang, P.-F., Yan, D.-H., Liao, N.-H., et al. 2017b, ApJ, 842, 10
Zhang, P.-F., Yan, D.-H., Zhou, J.-N., et al. 2017c, ApJ, 845, 82
Zhou, J., Wang, Z., Chen, L., et al. 2018a, Nat. Commun., 9, 4599
Zhou, J., Wang, Z., Chen, L., et al. 2018b, Nat. Commun., 9, 1
Zhou, X.-L., Yuan, W., Pan, H.-W., & Liu, Z. 2015, ApJ, 798, L5